HHS Public Access

Author manuscript

Adv Healthc Mater. Author manuscript; available in PMC 2018 September 01.

Published in final edited form as:

Adv Healthc Mater. 2017 September ; 6(18): . doi:10.1002/adhm.201700514.

Phospholipid Capped Mesoporous Nanoparticles for Targeted High Intensity Focused Ultrasound Ablation

Dr. Adem Yildirim,
Department of Chemical and Biological Engineering, University of Colorado Boulder. Boulder, Colorado 80303, United States

Rajarshi Chattaraj,
Department of Chemical and Biological Engineering, University of Colorado Boulder. Boulder, Colorado 80303, United States. Department of Mechanical Engineering, University of Colorado Boulder. Boulder, Colorado 80309, United States

Nicholas T. Blum,
Department of Chemical and Biological Engineering, University of Colorado Boulder. Boulder, Colorado 80303, United States

Dennis Shi, **Kaushlendra Kumar**, and
Department of Chemical and Biological Engineering, University of Colorado Boulder. Boulder, Colorado 80303, United States

Prof. Andrew P. Goodwin
Department of Chemical and Biological Engineering, University of Colorado Boulder. Boulder, Colorado 80303, United States

Abstract

The mechanical effects of cavitation can be effective for therapy but difficult to control, thus potentially leading to off-target side effects in patients. While administration of ultrasound active agents such as fluorocarbon microbubbles and nanodroplets can locally enhance the effects of high intensity focused ultrasound (HIFU), it has been challenging to prepare ultrasound active agents that are small and stable enough to accumulate in tumors and internalize into cancer cells. Here, we report the synthesis of 100 nm nanoparticle ultrasound agents based on phospholipid-coated, mesoporous, hydrophobically-functionalized silica nanoparticles that can internalize into cancer cells and remain acoustically active. The ultrasound agents produce bubbles when subjected to short HIFU pulses (~6 μs) with peak negative pressure as low as ~7 MPa and at particle concentrations down to 12.5 μg mL^{-1} (7×10^9 particles mL^{-1}). Importantly, ultrasound agents are effectively uptaken by cancer cells without cytotoxic effects, but HIFU insonation causes destruction of the cells by the acoustically generated bubbles, as demonstrated by XTT and LDH assays and flow cytometry. Finally, we showed that the HIFU dose required to effectively

Correspondence to: Adem Yildirim; Andrew P. Goodwin.

Supporting Information

Supporting Information is available from the Wiley Online Library or from the author.

eliminate cancer cells in the presence of ultrasound agents caused only a small temperature increase of ~3.5 °C.

Keywords

Mesoporous Silica; HIFU; Cancer Theranostics; Ultrasound Contrast Agents; Surface Science

High intensity focused ultrasound (HIFU) is a non-invasive ablation method that leverages the penetration depth and focusing of ultrasound at megahertz frequencies (~0.8–3.5 MHz) and has been investigated as an alternative to surgical resection of solid tumors,[1–3] as well as for direct treatment of Alzheimer's disease,[4] uterine fibroids,[3, 5] and kidney stones.[6, 7] HIFU utilizes ultrasound pulses with amplitudes that are several orders of magnitude greater than for standard diagnostic ultrasound but with low duty cycle. Thus, ultrasound waves pass through the surrounding tissues and selectively damage the focused region due to constructive interference of individual ultrasound waves at the focus, typically with millimeter resolution.[1, 8] Conventional, or thermal, HIFU therapy utilizes high acoustic doses with long pulses and high pulse repetition rates, generating a significant temperature increase (>50 °C) in the tissue that quickly induces protein denaturation, cell shrinkage, membrane destruction, and finally coagulation necrosis.[9, 10] While HIFU has been used for ablation of various solid tumors[3, 11–13] including breast, prostate, kidney, liver, bone, and pancreas, the therapeutic outcomes of current HIFU methods are still unsatisfactory due to the difficulties in obtaining the required high acoustic doses, especially for deep and hypervascularized tumors.[14, 15] Thus, recurrence after HIFU treatment is often observed for such tumors because of incomplete ablation.[10, 16] In addition, intense HIFU doses can damage the healthy tissue and cause off-target effects such as skin burns and nerve injury.[17, 18] More importantly, the volume of ablation after treatment with current HIFU methods is relatively large (typically cigar-shaped with dimensions on the order of 1–3 mm × 8–15 mm) and ablates tissue nonspecifically.[1] Thus, HIFU is often not suitable for treating small tumor nodules and micrometastases. Also, destruction of tumor vasculature during the HIFU treatment prevents the elimination of residual cancer cells by additional therapies such as chemotherapy or immunotherapy.[19]

Alternatively, shorter pulses with high acoustic pressures (>20 MPa) may be applied to induce mechanical effects by cavitation.[20, 21] Cavitation is the transient formation of a vapor pocket in liquid, which subsequently collapses to produce shock waves, water jets, and intense local temperature changes without causing a significant overall temperature change in the tissue on the macroscale.[22] However, the high acoustic pressure requirement to induce acoustic cavitation in the tissue is challenging to administer safely to deep tissue.[23] Colloidal ultrasound agents (microbubbles, nanodroplets, and others)[14, 24–32] can locally enhance the mechanical effects of HIFU due to nucleation of cavitation, resulting in formation of bubbles that can grow up to 100–200 μm before collapse.[33] Thus, application of targeted ultrasound agents may enable more precise elimination of cancer cells at much lower acoustic intensities and could thus address the above-mentioned limitations of current HIFU ablation methods. Current ultrasound contrast agents such as stabilized perfluorocarbon microbubbles or stabilized liquid droplets enhance both the mechanical and

thermal effects of HIFU to ablate larger lesions. However, because the Laplace pressure across the fluid interface requires a trade-off between size and stability, these colloids are usually too large (from 200 nm to a few microns) or unstable to effectively accumulate into the tumor and internalize into cancer cells.[30, 34]

In this communication, we report 100 nm, perfluorocarbon-free, robust, and biocompatible ultrasound agents based on phospholipid capped hydrophobic mesoporous silica nanoparticles (MSNs) that locally enhance the mechanical effects of HIFU inside cancer cells (Figure 1 a). We demonstrate that these ultrasound agents internalize into cancer cells, remain active after endocytosis, and eliminate the host cells when insonated with low HIFU doses. In addition, the progress and location of therapy may be monitored by imaging the generated bubbles during ablation using common ultrasound imaging equipment. Recently, we[34, 35] and others[36–40] showed that hydrophobic micro/nanoparticles dispersed in aqueous media can generate bubbles when subjected to an ultrasound pulse with peak negative pressures of a few MPa. Under reduced acoustic pressures, air stabilized at the hydrophobic interface act as nucleation sites for bubble growth. The bubble grows outside the particle from the contribution of the dissolved gases and water vapor, followed by collapse.[34, 37, 38] Such bubble generating micro/nanoparticles were applied to improve the contrast of ultrasound images by our group,[34, 35] and as well as to enhance the drug delivery efficiency by others.[37] Also, Zhao, *et al.,*[40] recently used hydrophobic MSNs to kill cancer cells by reactive oxygen species generation under continuous low energy ultrasound (LEUS) insonation rather than pulsed HIFU. However, inducing receptor-mediated uptake into cancer cells has remained largely unexplored, mainly due to the difficulties in functionalizing hydrophobic particles without diminishing their ability to generate bubbles by acoustic driving.[35, 38] Here, to create bubble-generating nanoparticles under reduced acoustic pressures with functionalizable surfaces, we coated phospholipid monolayers on hydrophobic MSNs to stabilize them in aqueous media. The hydrophobic interface stabilizes the air pockets needed for bubble generation[34, 35] and the phospholipid layer allows further functionalization with PEG and folic acid to improve dispersibility in biological media and facilitate their uptake by cancer cells, respectively.[41, 42]

The phospholipid stabilized MSNs were prepared using tetraethyl orthosilicate (TEOS) as the silica source, cetyltrimethylammonium chloride (CTAC) as the structure directing agent, and fluorescein isothiocyanate (FITC)-aminopropyltriethoxysilane (APTES) conjugate to fluorescently label the particles.[43] Transmission electron microscopy (TEM) revealed that the particles had an average diameter of 99 ± 17 nm with ~3 nm pores (Figure S1). The surface of the MSNs was then hydrophobically modified using dodecyltrichlorosilane. The dodecyl-modified MSNs (dMSN) were not dispersible in water (Figure S2a), which shows their strong hydrophobicity.[34, 44] Finally, the phospholipid monolayers were formed around the surface of dMSNs using a mixture of 1,2-dipalmitoyl-sn-glycero-3-phosphocholine (DPPC), 1,2-dipalmitoyl-sn-glycero-3-phosphate (sodium salt) (DPPA), 1,2-distearoyl-sn-glycero-3-phospho-ethanolamine-N-[methoxy (polyethylene glycol)-2000] (DSPE-PEG2k), and DSPE-PEG2k-folate (Figure S3).[45] The lipids assemble on the surface of the nanoparticles via hydrophobic-hydrophobic interactions between surface alkyl groups of dMSN and hydrophobic tails of phospholipids (Figure 1b).[45–47] DSPE-PEG2k was used to prevent agglomeration of the phospholipid stabilized particles[41] and DSPE-PEG2k-folate

was used to target MDA-MB-231 human breast adenocarcinoma.[42] The phospholipid stabilized particles (FA-PL-dMSN) were dispersible in PBS (Figure S2b). Nanoparticle tracking analysis (NTA) of FA-PL-dMSN indicated good dispersibility in PBS with an average particle size of 169 ± 47 nm (Figure 1c). In addition, NTA showed two major particle size populations around 125 and 170 nm with a shoulder around 260 nm. The latter peak and its shoulder are partially due to formation of some agglomerated dimers or trimers during synthesis (see the highlighted particles in Figure S1a). While the shoulder may be caused by the formation of some aggregates in PBS, because this peak was not as intense as other peaks, the particles were generally well-dispersed in PBS. The existence of phospholipid layers around the particles was confirmed by TEM with uranyl acetate negative staining.[46] While there was no contrast enhancement in the TEM images of unmodified MSN (Figure 1d and Figure S1c), bright layers were apparent around the FA-PL-dMSN (Figure 1e and Figure S1d). In addition, Fourier transform infrared (FTIR) spectroscopy verified the successful dodecyl and phospholipid modifications (Figure 1f). The intensity of CH_2 stretching and bending peaks at *ca.* 2950 and 1450 cm^{-1}[48, 49] increased after both dodecyl modification and phospholipid coating compared to unmodified MSNs, indicating increased organic content of the nanoparticles after each functionalization step. Integration of the CH_2 stretching peaks (between 2800 and 3000 cm^{-1}) of MSN, dMSN, and FA-PL-dMSN gave values of 4.7, 14.4, and 23.3 a.u., respectively. Next, thermogravimetric analysis (TGA) was performed to confirm the successful dodecyl and phospholipid modifications (Figure 1g). The weight loss between 150 and 600 °C was used to estimate the organic contents of the particles.[50] The percent weight loss in this region was 9.6% for unmodified MSNs, which is mostly attributed to the decomposition of fluorescein dye bonded to the silica network, removal of residual surfactant molecules, and loss of some hydroxyl groups.[50] The weight losses in this region were 15.8% for dMSN and 25.3% for FA-PL-dMSN, which were due to the additional dodecyl modification and phospholipid capping, respectively. Accordingly, dodecyl and phospholipid weight contents of FA-PL-dMSN were calculated to be 6.2% and 9.5%, respectively, which roughly correlate with the integrations in the FTIR spectra. These values are close to the expected weight of phospholipid only at the surface, which is consistent with other examples of phospholipid-coated silica nanoparticles.[51–53]

For control experiments, PEGylated MSN without hydrophobic modification was prepared by attaching PEG5k-NHS to the APTES-functionalized MSN surface.[54] Finally, folic acid was attached to the particle surface to promote cellular uptake; these particles are called FA-PEG-MSN. The successful PEGylation of the MSNs was confirmed by TEM and FTIR (Figure S4), and the nanoparticles' dispersibility in PBS was demonstrated using NTA measurements as described above. (Figure S5).

Formation of bubbles under HIFU insonation is easily observed by using an ultrasound imaging transducer since bubbles are good scatterers of ultrasound.[55] Image contrast was evaluated in the presence of FA-PL-dMSN as described in our previous reports (Figure S6a).[26, 34, 35, 56] Samples dispersed in PBS at different concentrations between 0 and 200 μg mL^{-1} were placed in a plastic tube with low acoustic attenuation, which was submerged in a water tank and placed on a HIFU transducer. A phased array scanning probe (Acuson 4V1) operating at 1.5 MHz in Cadence Contrast Pulse Sequencing (CPS) mode was aligned

in the x-direction to detect the generated bubbles when insonated with a HIFU transducer operating at 1.1 MHz. Since HIFU is applied in pulses, the total applied energy per volume per time is determined by the pulse intensity (W/cm^2), pulse duration (usually in the order of μs to ms), and pulse repetition frequency (usually Hz-kHz). The pulse intensity is proportional to the square of the peak pressure and the pulse duration and the time averaged intensity of HIFU linearly increases with increasing pulse repetition frequency.[57, 58]

In initial experiments, HIFU pulses with a duration of 10.9 μs at a peak negative pressure of 10.6 MPa were applied at a repetition frequency of 10 Hz. The FA-PL-dMSN sample (200 μg mL^{-1}) immediately produced bright spots corresponding to bubbles in the ultrasound images (Figure 2a). On the other hand, FA-PEG-MSN at the same particle concentration did not produce any contrast in the ultrasound images (Figure 2a), proving that a hydrophobic interface is required to stabilize air pockets for nucleation of bubbles under reduced acoustic pressures.[35] To quantify the ultrasound response of the particles, three 15 s videos were recorded for each sample and the brightness of the region of interest was quantified using MATLAB (Mathworks, Inc.). Figure 2b shows the ultrasound contrast intensity produced by the ultrasound agents at different concentrations. Phospholipid stabilized MSNs produced detectable ultrasound response at concentrations as low as 12.5 μg mL^{-1}, which corresponds to 7×10^9 particles mL^{-1} as determined by NTA measurements. Increasing the particle concentration from 12.5 to 100 μg mL^{-1} gradually increased the ultrasound contrast intensity but further increasing it to 200 μg mL^{-1} did not significantly affect the intensity. Accordingly, 100 μg mL^{-1} was determined as an optimum particle concentration and used in the rest of the study.

Next, we studied the effects of varying HIFU conditions on ultrasound contrast intensity generation by FA-PL-dMSN, starting with pulse duration (Figure 2c). Bubble formation was observed when the pulse duration was greater than ~5 μs; signal saturated when 10.9 μs pulses were applied. Next, the effect of peak negative pressure was studied at pulse duration of 10.9 μs. It was observed that FA-PL-dMSN generated bubbles when the peak negative pressure was >6.2 MPa, and signal saturated when HIFU was applied at 8.3 MPa or greater. Accordingly, peak negative pressure of 10.6 MPa and pulse duration of 10.9 μs were determined as optimum HIFU parameters for bubble generation by FA-PL-dMSN and used in the rest of the study. At these conditions, pulse intensity was calculated to be 720 W/cm^2[26] and duty cycle was only 0.011%.

After optimizing the conditions for bubble generation by FA-PL-dMSN, we studied their cyto-compatibility and cellular uptake using MDA-MB-231 human breast adenocarcinoma cells. According to (2,3-bis-(2-methoxy-4-nitro-5-sulfophenyl)-2H-tetrazolium-5-carboxanilide (XTT) and lactate dehydrogenase (LDH) assays (Figure 3a), no cytotoxicity was detected by the FA-PL-dMSN after 24 h incubation at concentrations up to 200 μg mL^{-1}. Next, cellular uptake of the FA-PL-dMSN was studied using flow cytometry and fluorescence microscopy at particle concentration of 100 μg mL^{-1}. Flow cytometry analysis of FITC-labelled FA-PL-dMSN showed their internalization into the MDA-MB-231 cells after overnight incubation (Figure 3b). In addition, cellular uptake of FA-PL-dMSN after 6 h incubation was observed by fluorescence microscopy (Figure S7). Because phospholipid coated MSNs without folic acid (PL-dMSN) showed almost no detectable uptake for these

particles after 6 h incubation (Figure S7), the uptake appeared to be mediated by the folate receptors. In addition, blocking the folate receptors by addition of free folic acid (2 mM) 2 h prior to the FA-PL-dMSN addition significantly reduced the nanoparticle uptake (Figure S7), further proving folate receptor mediated uptake.[42] The good cytocompatibility and efficient cellular uptake was also observed for FA-PEG-MSN; non-responsive control particles (Figure S8).

To determine if the ultrasound agents remained active after cellular internalization, we incubated the FA-PL-dMSN with MDA-MB-231 cells overnight. The cells were washed extensively with PBS to remove free particles, and cells were collected by trypsinization and dispersed in fresh media (5×10^5 cells mL^{-1}). At the HIFU conditions described above, signal could be observed from the cell suspension (Figure 3c). This procedure demonstrates the stability of the ultrasound agents after cell uptake (see also Video S1). In the absence of pre-incubation with ultrasound agents, on the other hand, cells did not produce any ultrasound signal (Figure 3c).

Next, cellular damage induced by bubble generation in the presence of internalized ultrasound agents was investigated using a lactate dehydrogenase (LDH) assay, which screens for damage to cell membranes. First, MDA-MB-231 cells were grown in 6 well plates for 1 d and media was replaced with media containing nanoparticles (FA-PL-dMSN, PA-PEG-MSN, or none). After incubation overnight, the cells were collected by trypsinization, suspended in fresh media, and added to 96 well plates (10^4 cells per well). Plates were placed on a HIFU cone in a water tank and each well was insonated for 30 s at the HIFU parameters determined above (pulse duration of 10.9 μs and peak negative pressure of 10.6 MPa), using different pulse repetition frequencies between 1 Hz and 2 kHz (corresponding duty cycles are between ~0.001% and 2.2%) (Figure S6b). It was observed that FA-PL-dMSN caused cellular damage even at a very low pulse repetition frequency of 1 Hz (Figure 4a). These HIFU conditions correspond to only ~30 pulses in 30 s and a duty cycle of ~0.001%. Cellular damage was increased with increasing repetition frequency, reaching *ca.* 40% at 0.5 kHz. The cellular damage in the presence of FA-PEG-MSN or for HIFU only was much lower compared to the FA-PL-dMSN, showing only 8% and 2% at 0.5 kHz, respectively. The cellular viability after HIFU treatment was also studied using a XTT assay (Figure 4b). While the decrease in the cellular viabilities up to 0.5 kHz was not statistically different than the control, at 0.5 kHz a large decrease (~60%) in the viability was observed for FA-PL-dMSN. With non-responsive FA-PEG-MSN nanoparticles, or no nanoparticles at all, significant cell death was not observed, which was consistent with LDH assay results. Increasing the pulse repetition frequency to 2 kHz resulted in significant cell death for all conditions as determined by LDH and XTT assays (Figure 4a,b). Nevertheless, cellular damage was higher for FA-PL-dMSN, where cells were almost completely eliminated. To determine if cell death was more likely due to thermal or cavitation effects, the temperature increase after HIFU treatment was measured at different pulse repetition frequencies in the presence or absence of FA-PL-dMSN (Figure 4c). No temperature increase was observed when the pulse repetition frequency was lower than 0.1 kHz. Small temperature increases of 1 °C and ~3.5 °C were observed after insonating the wells at 0.1 and 0.5 kHz, respectively. Thus, cell death at repetition frequencies 0.1 kHz or less were likely purely mechanical. For 2 kHz repetition frequency, the temperature increased *ca.*

11 °C, corresponding to significant cellular damage for types of particles. Because a similar temperature increase was observed regardless of particle addition, the temperature increase is likely due to absorption of HIFU acoustic energy by the aqueous medium (Figure 4c).[1] These results suggest that cells can be eliminated by the local mechanical effects generated by cavitating bubbles, not just by a large and rapid temperature increase in the surrounding environment.

Finally, flow cytometry was applied to investigate the effects of HIFU and the ultrasound agents on MDA-MB-231 cells. HIFU exposure can affect the cells in different ways. First, the generated bubbles can ablate the cells or induce cell death due to irreversible membrane damage. Second, the bubbles may cause reversible cell membrane damage, referred to as sonoporation. Finally, nothing could happen to the cells at all. For flow cytometry experiments, 150 μM propidium iodide (PI) was added to each well before HIFU treatment to label dead or sonoporated cells, and cells were insonated with HIFU for 30 s at different pulse repetition frequencies. Figure 4d shows the scatterplot of forward scatter (FSC) vs. PI fluorescence analysis of the cells, in which we identified four distinct regions.[59] The cells in Region I are considered viable cells because they have larger size as determined by FSC and low PI fluorescence intensity. The cells in Region II are viable sonoporated cells because they have both large sizes and high PI fluorescence intensity. Region III is attributed to dead cells due to the reduced cell size and high PI fluorescence intensity, both of which are indicators of cell death. Finally, the recorded events in Region IV indicate cell debris, a sign of cell ablation. Figure 4e summarizes the percentages in each region after HIFU treatment at different pulse repetition frequencies in the presence of FA-PL-dMSN. With increasing pulse repetition frequency, the fraction of cells in Region I decreases but the fractions in the other regions increase, indicating that administration of HIFU in the presence of FA-PL-dMSN induces both cell ablation (Region IV), death (Region III), and sonoporation (Region II). Nevertheless, the number of sonoporated cells was very low (4% at 0.5 kHz) compared to the ablated and dead cells. Also, the decrease in the number of viable cells was more than 50% for the cells treated at 0.5 kHz, which is in accordance with the LDH and XTT results. Finally, increase in the number of dead cells was very small when the cells were treated with only HIFU or FA-PEG-MSN at 0.5 kHz (Figure S9), further proving that cancer cell ablation and death is enhanced by the bubble generation ability of internalized FA-PL-dMSN under HIFU insonation.

In summary, we developed novel nanoscale ultrasound agents based on phospholipid-capped, hydrophobic MSNs. We showed that these robust ultrasound agents internalize into cancer cells and eliminate them when exposed to low doses of HIFU without causing a significant temperature increase. The ultrasound agents produced bubbles when exposed to HIFU, at a low particle concentration of ~7×10^9 particles mL^{-1}. The ablation of cancer cells by the generated bubbles was demonstrated using LDH and XTT assays and flow cytometry. With their small size, good biocompatibility, functionalizable surfaces, and excellent stability in biological media, these ultrasound agents can effectively accumulate in tumors and ablate the target cancer cells with minimal damage to the surrounding tissue and vasculature and, thus can improve the therapeutic outcomes of HIFU based methods.

Supplementary Material

Refer to Web version on PubMed Central for supplementary material.

Acknowledgments

The authors thank NIH (R03EB021432 and DP2EB020401) for funding. The authors would like to acknowledge Prof. Amy Palmer for use of her cell plate reader, Prof. Stephanie Bryant for use of her cell culture equipment, Prof. Jeffrey Stansbury for use of his Thermo Scientific Nicolet 6700 FTIR and Perkin Elmer Pyris 1 TGA, Dr. Luke Amer for cell culture training, Theresa Nahreini for her help with flow cytometry, and Prof. Jennifer Cha for helpful discussions.

References

1. Kennedy JE. Nat Rev Cancer. 2008; 5:321.
2. Kennedy JE, ter Haar GR, Cranston D. Br J Radiol. 2003; 76:590. [PubMed: 14500272]
3. Al-Bataineh O, Jenne J, Huber P. Cancer Treat Rev. 2012; 38:346. [PubMed: 21924838]
4. Leinenga G, Goetz J. Sci Transl Med. 2015; 7:11.
5. Zhanga L, Chena WZ, Liub YJ, Hub X, Zhoua K, Chenb L, Penga S, Zhua H, Zoub HL, Baic J, Wang ZB. Eur J Radiol. 2010; 73:396. [PubMed: 19108974]
6. Ikeda T, Yoshizawa S, Tosaki M, Allen JS, Takagi S, Ohta N, Kitamura T, Matsumoto Y. Ultrasound Med Biol. 2006; 32:1383. [PubMed: 16965979]
7. Sorensen MD, Bailey MR, Hsi RS, Cunitz BW, Simon JC, Wang YN, Dunmire BL, Paun M, Starr F, Lu W, Evan AP, Harper JD. J Endourol. 2013; 27:1183. [PubMed: 23883117]
8. Poissonnier L, Chapelon JY, Rouvière O, Curiel L, Bouvier R, Martin X, Dubernard JM, Gelet A. Eur Urol. 2007; 51:381. [PubMed: 16857310]
9. Manthe RL, Foy SP, Krishnamurthy N, Sharma B, Labhasetwar V. Mol Pharm. 2010; 7:1880. [PubMed: 20866097]
10. Zhang X, Zheng Y, Wang Z, Huang S, Chen Y, Jiang W, Zhang H, Ding M, Li Q, Xiao X, Luo X, Wang Z, Qi H. Biomaterials. 2014; 35:5148. [PubMed: 24680663]
11. Wu F, Wang ZB, Zhu H, Chen WZ, Zou JZ, Bai J, Li KQ, Jin CB, Xie FL, Su HB. Radiology. 2005; 236:1034. [PubMed: 16055692]
12. Schmitz AC, Gianfelice D, Daniel BL, Mali W, van den Bosch M. Eur Radiol. 2008; 18:1431. [PubMed: 18351348]
13. Wu F, Wang Z-B, Cao Y-D, Zhu X-Q, Zhu H, Chen W-Z, Zou J-Z MD . J Surg Oncol. 2007; 96:130. [PubMed: 17443737]
14. Liberman A, Wu Z, Barback CV, Viveros RD, Wang J, Ellies LG, Mattrey RF, Trogler WC. J Surg Res. 2014; 190:391. [PubMed: 24972734]
15. Choi SY, Kim YS, Seo YJ, Yang J, Choi KS. Plos One. 2012; 7:e34333. [PubMed: 22479602]
16. Yao M, Ma M, Chen Y, Jia X, Xu G, Xu HX, Chen HR, Wu R. Biomaterials. 2014; 35:8197. [PubMed: 24973300]
17. Zhang N, Cai X, Gao W, Wang R, Xu C, Yao Y, Hao L, Sheng D, Chen H, Wang Z, Zheng Y. Theranostics. 2016; 6:404. [PubMed: 26909114]
18. Wang S, Zhao J, Hu F, Li X, An X, Zhou S, Chen Y, Hunag M. J Mater Chem B. 2016; 4:46.
19. Bandyopadhyay S, Quinn TJ, Scandiuzzi L, Basu I, Partanen A, Tomé WA, Macian F, Guha C. J Immunol. 2016; 196:1964. [PubMed: 26755821]
20. Vlaisavljevich E, Kim Y, Allen S, Owens G, Pelletier S, Cain C, Ives K, Xu Z. Ultrasound Med Biol. 2013; 39:1398. [PubMed: 23683406]
21. Aydin O, Vlaisavljevich E, Durmaz YY, Xu Z, ElSayed MEH. Mol Pharm. 2016; 13:4054. [PubMed: 27696857]
22. Morch KA. Phys Fluids. 2007; 19:072104.
23. Vlaisavljevich E, Durmaz YY, Maxwell A, ElSayed M, Xu Z. Theranostics. 2013; 3:851. [PubMed: 24312155]

24. Hsieh CC, Kang ST, Lin YH, Ho YJ, Wang CH, Yeh CK, Chang CW. Theranostics. 2015; 5:1264. [PubMed: 26379791]
25. Chen Y, Chen HR, Shi JL. Adv Healthcare Mater. 2015; 4:8.
26. Blum NT, Yildirim A, Chattaraj R, Goodwin AP. Theranostics. 2017; 7:694. [PubMed: 28255360]
27. Ma M, Xu H, Chen H, Jia X, Zhang K, Wang Q, Zheng S, Wu R, Yao M, Cai X, Li F, Shi J. Adv Mater. 2014; 26:7378. [PubMed: 25228225]
28. Wang X, Chen H, Chen Y, Ma M, Zhang K, Li F, Zheng Y, Zeng D, Wang Q, Shi J. Adv Mater. 2012; 24:785. [PubMed: 22223403]
29. Wang X, Chen H, Zhang K, Ma M, Li F, Zeng D, Zheng S, Chen Y, Jiang L, Xu H, Shi J. Small. 2014; 10:1403. [PubMed: 24288148]
30. Zhou Y, Wang Z, Chen Y, Shen H, Luo Z, Li A, Wang Q, Ran H, Li P, Song W, Yang Z, Chen H, Wang Z, Lu G, Zheng Y. Adv Mater. 2013; 25:4123. [PubMed: 23788403]
31. Chattaraj R, Goldscheitter GM, Yildirim A, Goodwin AP. RSC Adv. 2016; 6:111318. [PubMed: 28603605]
32. Wang CH, Kang ST, Lee YH, Luo YL, Huang YF, Yeh CK. Biomaterials. 2012; 33:1939. [PubMed: 22142768]
33. Kwan JJ, Lajoinie G, de Jong N, Stride E, Versluis M, Coussios CC. Phys Rev Applied. 2016; 6:044004.
34. Yildirim A, Chattaraj R, Blum NT, Goldscheitter GM, Goodwin AP. Adv Healthcare Mater. 2016; 5:1290.
35. Yildirim A, Chattaraj R, Blum NT, Goodwin AP. Chem Mater. 2016; 28:5962. [PubMed: 28484307]
36. Kwan JJ, Graham S, Myers R, Carlisle R, Stride E, Coussios CC. Phys Rev E. 2015; 92:023019.
37. Kwan JJ, Myers R, Coviello CM, Graham SM, Shah AR, Stride E, Carlisle RC, Coussios CC. Small. 2015; 39:5305.
38. Jin QF, Kang ST, Chang YC, Zheng HR, Yeh CK. Inertial cavitation initiated by polytetrafluoroethylene nanoparticles under pulsed ultrasound stimulation (in English). Ultrason Sonochem. 2016; 32:1. [PubMed: 27150739]
39. Zhang L, Belova V, Wang HQ, Dong WF, Mohwald H. Chem Mater. 2014; 26:244.
40. Zhao Y, Zhu Y, Fu J, Wang L. Chem Asian J. 2014; 9:790. [PubMed: 24339016]
41. Rausch K, Reuter A, Fischer K, Schmidt M. Biomacromolecules. 2010; 11:2836. [PubMed: 20961117]
42. Yang H, Li Y, Li T, Xu M, Chen Y, Wu C, Dang X, Liu Y. Sci Rep. 2014; 4:7072. [PubMed: 25400232]
43. Liong M, Lu J, Kovochich M, Xia T, Ruehm SG, Nel AE, Tamanoi F, Zink JI. ACS Nano. 2008; 2:889. [PubMed: 19206485]
44. Yildirim A, Demirel GB, Erdem R, Senturk B, Tekinay T, Bayindir M. Pluronic polymer capped biocompatible mesoporous silica nanocarriers (in English). Chem Commun. 2013; 49:9782.
45. Teng IT, Chang YJ, Wang LS, Lu HY, Wu LC, Yang CM, Chiu CC, Yang CH, Hsu SL, Ho JA. Biomaterials. 2013; 34:7462. [PubMed: 23810081]
46. Wang LS, Wu LC, Lu SY, Chang LL, Teng IT, Yang CM, Ho JA. ACS Nano. 2010; 4:44371.
47. Prencipe G, Tabakman SM, Welsher K, Liu Z, Goodwin AP, Zhang L, Henry J, Dai H. J Am Chem Soc. 2009; 131:4783. [PubMed: 19173646]
48. Guo C, Liu HZ, Wang J, Chen JY. Conformational structure of triblock copolymers by FT-Raman and FTIR spectroscopy. J Colloid Interface Sci. 1999; 209:368. [PubMed: 9885264]
49. Su YL, Wang J, Liu HZ. Langmuir. 2002; 18:5370.
50. Kim JM, Chang SM, Kong SM, Kim KS, Kim J, Kim WS. Ceram Int. 2009; 35:1015.
51. Ahmed S, Wunder SL. Langmuir. 2009; 25:3682. [PubMed: 19231878]
52. Ashley CE, Carnes EC, Phillips GK, Padilla D, Durfee PN, Brown PA, Hanna TN, Liu J, Phillips Brandy, Carter MB, Carroll NJ, Jiang X, Dunphy DR, Willman CL, Petsev DN, Evans DG, Parikh AN, Chackerian B, Wharton W, Peabody DS, Brinker CJ. Nat Mater. 2011; 10:389. [PubMed: 21499315]

53. Liu J, Stace-Naughton A, Jiang X, Brinker CJ. J Am Chem Soc. 2009; 131:1354. [PubMed: 19173660]
54. Lee SB, Kim HL, Jeong HJ, Lim ST, Sohn MH, Kim DW. Angew Chem In Ed. 2013; 52:10549.
55. Schutt EG, Klein DH, Mattrey RM, Riess JG. Angew Chem In Ed. 2003; 42:3218.
56. Chattaraj R, Mohan P, Besmer JD, Goodwin AP. Adv Healthcare Mater. 2015; 4:1790.
57. Harris GR. Ultrasound Med Biol. 1985; 11:803. [PubMed: 3913079]
58. Kieran K, Hall TL, Parsons JE, Wolf JS, Fowlkes JB, Cain CA, Roberts WW. J Urol. 2007; 178:672. [PubMed: 17574617]
59. Schlicher RK, Hutcheson JD, Radhakrishna H, Apkarian RP, Prausnitz MR. Ultrasound Med Biol. 2010; 36:677. [PubMed: 20350691]

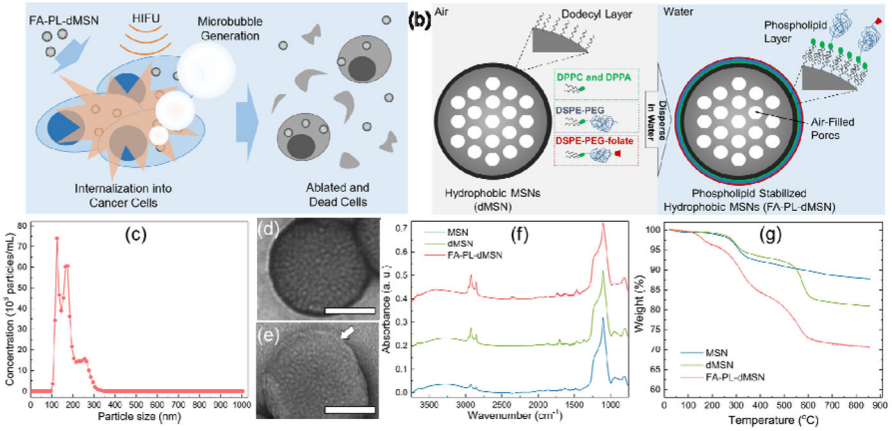

Figure 1.

Design and characterization of nanoscale ultrasound agents. a) Schematic representation of microbubble generation and cancer cell elimination by phospholipid coated mesoporous silica nanoparticles upon HIFU exposure. b) Schematic representation of phospholipid coated mesoporous silica nanoparticle preparation. c) Size distribution of FA-PL-dMSN in PBS (pH 7.4, 10 mM) as determined by Nanoparticle Tracking Analysis. TEM images of d) MSN and e) FA-PL-dMSN with uranyl acetate stain. Arrow in e) indicate the phospholipid layer around the MSNs. f) FTIR spectra of MSN, dMSN, and FA-PL-dMSN. g) TGA spectra of MSN, dMSN, and FA-PL-dMSN. Scale bars in (d) and (e) are 50 nm.

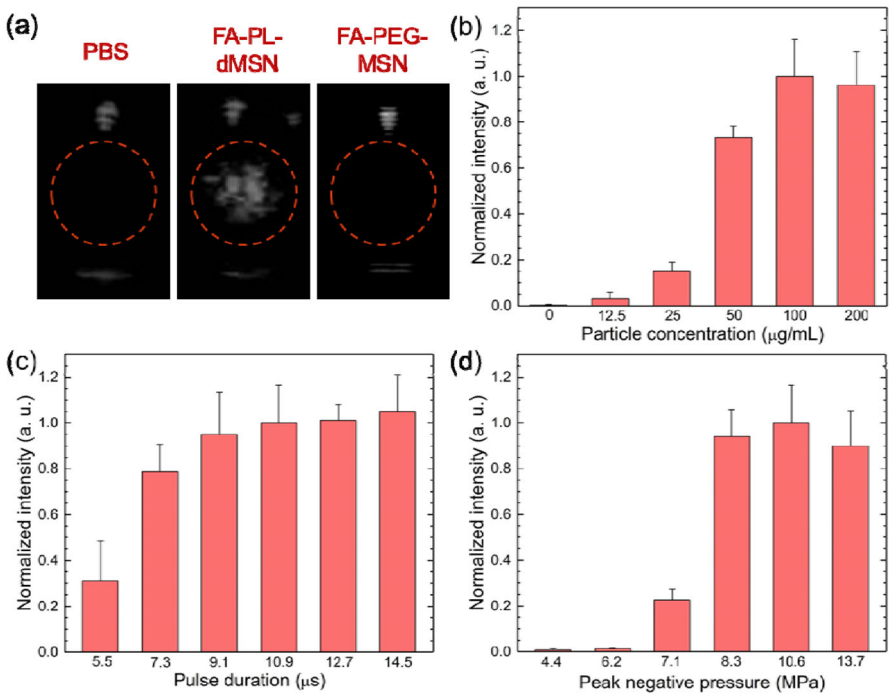

Figure 2.

Microbubble generation by nanoscale ultrasound agents upon HIFU exposure. a) Representative images were taken from movies acquired during HIFU irradiation in the presence or absence of nanoparticles (200 μg mL^{-1}). Microbubble generation was only observed in the presence of FA-PL-dMSN. b) Normalized ultrasound contrast intensities from the acquired movies of FA-PL-dMSN samples at different concentrations were exposed to HIFU at a pulse duration of 10.9 μs and peak negative pressure of 10.6 MPa. c) Normalized ultrasound contrast intensities from the acquired movies of FA-PL-dMSN samples (100 μg mL^{-1}) were exposed HIFU with different pulse durations at a peak negative pressure of 10.6 MPa. d) Normalized ultrasound contrast intensities from the acquired movies of FA-PL-dMSN samples (100 μg mL^{-1}) were exposed to HIFU with different peak negative pressures at pulse duration of 10.9 μs. Error bars = 1 SD, studies were run in triplicate.

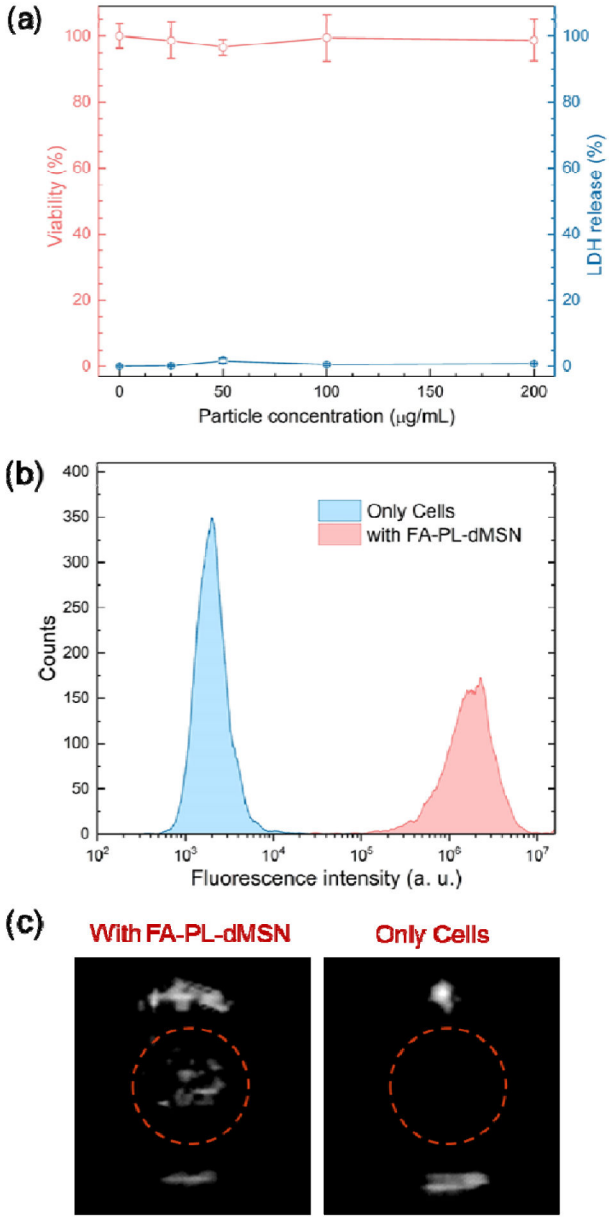

Figure 3.

Cytocompatibility, uptake, and stability of the nanoscale ultrasound agents. a) XTT and LDH assays for the MDA-MB-231 cells which were incubated with FA-PL-dMSN at different concentrations for 24 h. b) Uptake of FITC labelled FA-PL-dMSN (100 μg mL^{-1}) by MDA-MB-231 cells as determined by flow cytometry. c) Still images of the typical ultrasound contrast generated by MDA-MB-231 cell suspensions (5×10^5 cells mL^{-1}) pre-incubated with or without FA-PL-dMSN (200 μg mL^{-1}) for overnight upon HIFU (pulse duration 10.9 μs and peak pressure 10.6 MPa) exposure. Error bars = 1 standard error of the mean (SEM), studies were run in triplicate.

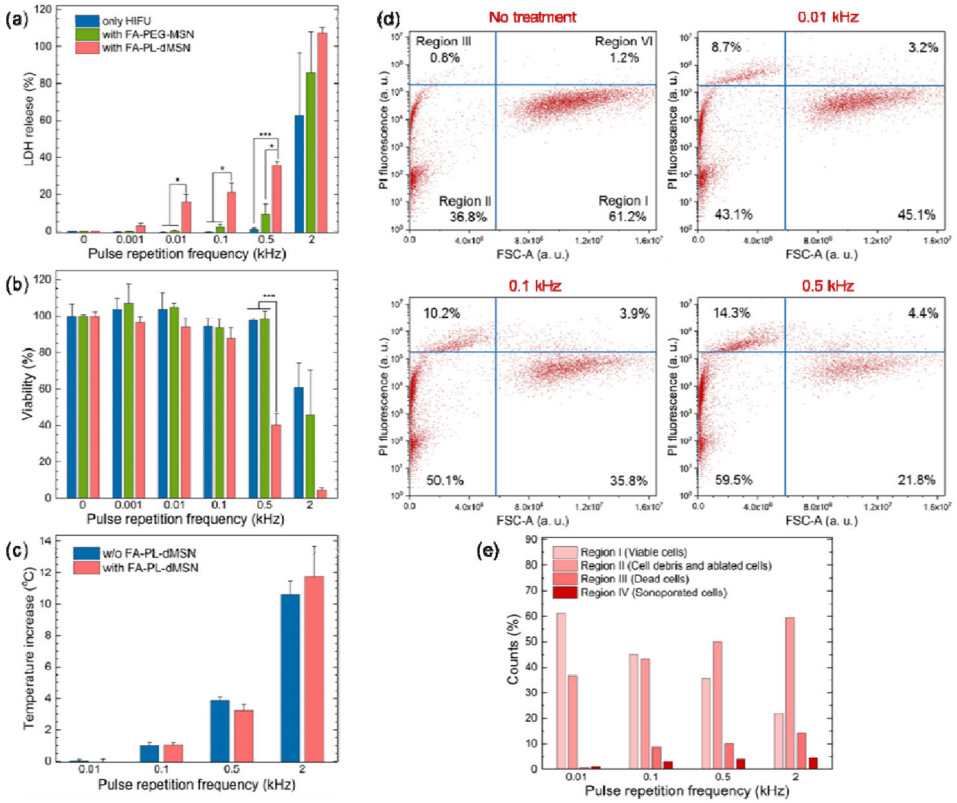

Figure 4.

Cellular damage by the internalized ultrasound agents after HIFU insonation. a) LDH and b) XTT assays of MDA-MB-231 cells, which were pre-incubated with or without FA-PL-dMSN (100 μg mL^{-1}) or FA-PEG-MSN (100 μg mL^{-1}) overnight, followed by 30 s HIFU exposure (pulse duration of 10.9 μs, 10.6 MPa) at different pulse repetition frequencies. c) Temperature raise of PBS containing or not containing FA-PL-dMSN (100 μg mL^{-1}) after 30 s of HIFU exposure (pulse duration of 10.9 μs, 10.6 MPa) at different pulse repetition frequencies. d) Propidium iodide (PI) fluorescence versus Forward Scatter-Area (FSC-A) plots of the MDA-MB-231 cells pre-incubated with FA-PL-dMSN (100 μg mL^{-1}) for overnight and exposed to after HIFU (pulse duration of 10.9 μs, 10.6 MPa) for 30 s at different pulse repetition frequencies. We defined four regions in the flow cytometry plots; viable cells (region I), ablated cells (region II), dead cells (region III), and sonoporated cells (region IV). e) Graph showing counts (%) for each region in the flow cytometry plot in d). Error bars = 1 standard error of the mean (SEM) for a) and b) and 1 SD for c), studies were run in triplicate. According to Student's t-test, *$p < 0.05$ and ***$p < 0.0001$.